CHEMISTRY
A EUROPEAN JOURNAL

FULL PAPER

DOI: 10.1002/chem.201303123

Solvent-Induced Helical Assembly and Reversible Chiroptical Switching of Chiral Cyclic-Dipeptide-Functionalized Naphthalenediimides

Shivaprasad Manchineella,[a] V. Prathyusha,[b] U. Deva Priyakumar,*[b] and T. Govindaraju*[a]

Abstract: Understanding the roles of various parameters in orchestrating the preferential chiral molecular organization in supramolecular self-assembly processes is of great significance in designing novel molecular functional systems. Cyclic dipeptide (CDP) chiral auxiliary-functionalized naphthalenediimides (NCDPs **1**–**6**) have been prepared and their chiral self-assembly properties have been investigated. Detailed photophysical and circular dichroism (CD) studies have unveiled the crucial role of the solvent in the chiral aggregation of these NCDPs. NCDPs **1**–**3** form supramolecular helical assemblies and exhibit remarkable chiroptical switching behaviour (*M*- to *P*-type) depending on the solvent composition of HFIP and DMSO. The strong influence of solvent composition on the supramolecular chirality of NCDPs has been further corroborated by concentration and solid-state thin-film CD studies. The chiroptical switching between supramolecular aggregates of opposite helicity (*M* and *P*) has been found to be reversible, and can be achieved through cycles of solvent removal and redissolution in solvent mixtures of specific composition. The control molecular systems (NCDPs **4**–**6**), with an achiral or D-isomer second amino acid in the CDP auxiliary, did not show chiral aggregation properties. The substantial roles of hydrogen bonding and π–π interactions in the assembly of the NCDPs have been validated through nuclear magnetic resonance (NMR), photophysical, and computational studies. Quantum chemical calculations at the ab initio, semiempirical, and density functional theory levels have been performed on model systems to understand the stabilities of the right (*P*-) and left (*M*-) handed helical supramolecular assemblies and the nature of the intermolecular interactions. This study emphasizes the role of CDP chiral auxiliaries on the solvent-induced helical assembly and reversible chiroptical switching of naphthalenediimides.

Keywords: chiroptical switching · circular dichroism · cyclic dipeptides · naphthalenediimides · self-assembly · supramolecular chirality

Introduction

Helical chirality is ubiquitous in biological systems, as seen in DNA and proteins.[1] The helical conformations adopted by synthetic oligomers and polymers are pertinent to various applications, such as chiral recognition, asymmetric catalysis, chiral separation, and chiroptical switching.[2] In recent times, helical chirality in supramolecular polymers has attracted considerable interest due to the intrinsic dynamic nature of such materials and the ease with which their structural and functional properties may be tuned compared to covalent polymers.[3] The characteristic feature of such supramolecular polymers is the assembly of π-conjugated and aromatic monomer units with stabilization through hydrogen bonding and π-stacking interactions. Induction of helical chirality in supramolecular polymers through structural variations at the molecular self-assembly level is challenging due to the interplay of multiple noncovalent interactions. In general, the noncovalent synthesis of supramolecular polymers can be modulated through external stimuli capable of influencing the mode of molecular self-assembly. In this context, previous literature reports suggest that helical handedness in a self-assembly system can be achieved by employing similar external stimuli and chiral auxiliaries.[4] External stimuli such as temperature, light, solvent, and additives have been successfully used to control the chiral handedness of synthetic oligomers and polymers.[5–8] Some of the successful reports on chiral modulation in noncovalent systems have dealt with solvent-modulated supramolecular chirality of merocyanines, squarine dyes, and benzenetricarboxylic acid derivatives.[9–11]

Naphthalenediimide (NDI), the bis-imide derivative of 1,4,5,8-naphthalenetetracarboxylic dianhydride (NDA), is an

[a] S. Manchineella, Dr. T. Govindaraju
Bioorganic Chemistry Laboratory, New Chemistry Unit
Jawaharlal Nehru Centre for Advanced Scientific Research
Jakkur, Bangalore 560064 (India)
Fax: (+91) 80-2208-2627
E-mail: tgraju@jncasr.ac.in

[b] V. Prathyusha, Dr. U. D. Priyakumar
Centre for Computational Natural Sciences and Bioinformatics
International Institute of Information Technology
Hyderabad 500032 (India)
E-mail: deva@iiit.ac.in

Supporting information for this article is available on the WWW under http://dx.doi.org/10.1002/chem.201303123: Synthetic procedures and characterization of NCDP **1**–**6**, experimental details, UV/Vis absorption, emission, and CD data, theoretical calculations, and models of NCDPs.

extremely useful molecular platform with applications ranging from organic electronics to biomedicine.[12] The possibility of selective imide functionalization, high π-acidity, planarity conducive to strong π–π interactions, and ease of processability of these systems in solution has led to increased demand for the design of novel NDI-based supramolecular systems. Imide substituents studied have included alkyl chains, aromatic rings, amino acids, dipeptides, and a combination of alkyl chains and amino acids.[13–21] Our recent work demonstrated the potential of a biomimetic strategy based on amino acid- and peptide-functionalized NDIs for designing 0D, 1D, and 2D molecular materials with interesting structural and functional properties.[12e,20,21] The functional relevance of these biomimetic molecular materials varied from attolitre containers for miniaturized biological assays to organic electronics to self-cleaning functional molecular materials.[12e,20] Furthermore, the amino acid- and dipeptide-functionalized NDIs emphasized the significance of the chiral centre of the amino acid directly attached to the imide nitrogen in controlling the supramolecular helical chirality of the derived self-assembled structures.[21] Subsequently, the chiroptical properties of these systems revealed significant chiral transcription, amplification, and retentive helical memory with probable implications for the origin of homochirality in Nature.[1c]

Cyclic dipeptides (CDPs) are the smallest possible cyclic forms of peptides and are known for their unique structural properties and diverse biological functions.[22] By virtue of their structural rigidity, propensity for strong intermolecular hydrogen bonding, molecular recognition, and resistance towards proteolytic enzymes, CDPs constitute good supramolecular synthons for the preparation of soft organogels, hydrogels, and well-defined nanoarchitectures for various applications.[23–25] We envisaged an inclusive molecular design based on NDI with CDP chiral auxiliaries as monomers for the noncovalent synthesis of helical supramolecular polymers. The NDI-CDP (NCDP) conjugates serve as model systems to evaluate the role of chiral centres on the imide substituents located several atoms away from the imide nitrogen in inducing specific helical assemblies of NDI. This study complements our earlier work, in which the chiral centre of the first amino acid directly attached as the imide substituent through the α-amino group was found to determine the outcome of the helical assembly of NDIs.[20,21] The NCDP molecular platform has also assisted our understanding of the influence of α-substituents and the corresponding chiral centres in CDP auxiliaries. Herein, we report novel symmetrical NCDPs (**1–6**) as new molecular platforms to engineer NDI chiral assembly through aromatic (NDI) and hydrogen-bonding (CDP) interactions. Furthermore, this study emphasizes the significance of chiral auxiliaries and the decisive role played by solvent composition in modulating the helical supramolecular self-assembly of such systems.

Results and Discussion

We synthesized CDPs [cyclo(L-Lys-L-Tyr), cyclo(L-Lys-L-Phe), cyclo(L-Lys-L-Leu), cyclo(L-Lys-Gly), cyclo(L-Lys-D-Tyr), and cyclo(L-Lys-D-Phe)] from the corresponding linear dipeptides, retaining L-lysine as one of the amino acids and varying the second amino acid to obtain α-substituents with the required stereochemistry (Figure 1).[24a] These CDP auxiliaries were condensed with NDA through the ε-amine group of lysine to obtain NCDPs **1–6**, respectively, in good to excellent yields (Schemes S1–S6 in the Supporting Information). All of the NCDPs were characterized by NMR spectroscopy, elemental analysis, and mass spectrometry. Ini-

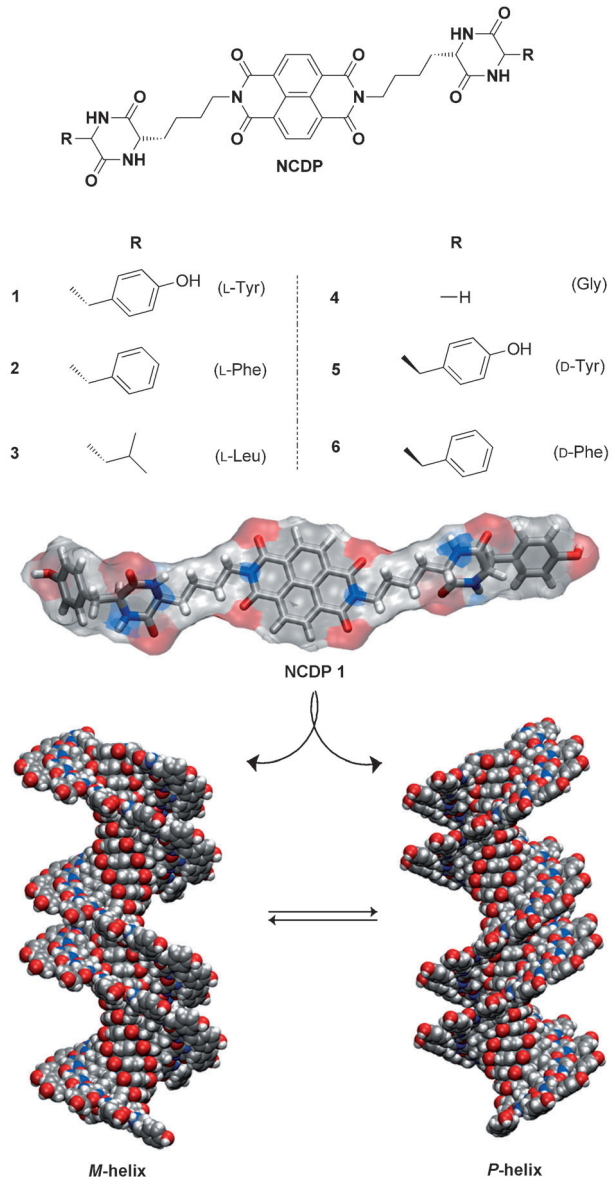

Figure 1. Top: Molecular structures of naphthalenediimides with different CDP auxiliaries (NCDPs **1–6**). Bottom: Model of monomer NCDP **1** and its *M*-helical and *P*-helical organization in HFIP and DMSO/HFIP, respectively.

tially, we chose NCDP **1** with L-tyrosine as the second amino acid of the CDP auxiliary for our detailed study owing to the characteristic self-assembling properties of L-tyrosine when present in polymer chains and the strong intermolecular interactions among cyclo(L-Tyr-L-Lys) derivatives.[25] The molecular interactions and chiral aggregation properties of NCDP **1** were studied by UV/Vis absorption and CD spectroscopic measurements in 1,1,1,3,3,3-hexafluoroisopropanol (HFIP), dimethyl sulfoxide (DMSO), and mixtures thereof. Specifically, HFIP is known to stabilize helical conformations in peptides through various mechanisms.[26]

The high solvent polarity, hydrogen-bond accepting properties, and localized hydrophobic solvating effects of methyl groups in DMSO are thought to facilitate solvatophobic interactions, thereby inducing aggregation in binary solvent mixtures through diverse mechanisms.[27] NCDP **1** (100 μM) in HFIP showed absorption peaks in the region 300–400 nm, a characteristic band I absorption for NDI. The corresponding emission spectrum showed weak fluorescence characteristic of amino acid-functionalized NDIs.[20,21] NCDP **1** exhibited aggregation-induced self-assembly with increasing volume fraction of DMSO (0–30%) in HFIP. A strong hypochromic effect and a slight hypsochromic shift were observed for the NDI absorption band (300–400 nm) (Figure 2a). CD studies were performed to gain insight into the chiroptical properties of NCDP **1**. In HFIP at lower concentrations (<100 μM), NCDP **1** did not show CD signals. However, a monosignate negative CD signal was obtained upon increasing the concentration of the solution to 100 μM, indicating *M*-helical (left-handed) assembly of NCDP **1** (Figure 2b). Negative Cotton signals were consistently observed for all concentrations of the solution (100–500 μM), indicating no interference with the chiral aggregation due to concentration effects. Furthermore, it should be noted that the CD spectra on the molar ellipticity scale (data not shown) showed similar CD signal intensity, which clearly demonstrated that the chiroptical switching was independent of concentration. The observed *M*-helical bias of NCDP **1** may be ascribed to the aggregation of molecules (≥100 μM) and preferential stabilization of one of the helical forms (*M*-type) by HFIP. It is presumed that in HFIP the *M*-helical assembly is the thermodynamically preferred arrangement of NCDP **1**. Semiempirical quantum chemical and density functional theory calculations on model structures were used to examine the relative stabilities of *M*- and *P*-helical assemblies, as discussed later.

Furthermore, we studied the effect of DMSO/HFIP solvent composition on the chiral aggregation of NCDP **1**. CD spectra of NCDP **1** (500 μM) were recorded as a function of increasing volume fraction of DMSO (v/v) in HFIP. There was no change in the negative Cotton signal upon increasing the volume fraction of DMSO up to 10% (v/v) in HFIP. Surprisingly, however, the negative Cotton signal was transformed completely to a bisignate positive Cotton signal at volume fractions of DMSO >10% in HFIP, indicating a reversal of chiral assembly from *M*- to *P*-helicity (right-handed). At 15% DMSO in HFIP (15:85, v/v), NCDP **1** exhibited maximum CD signal intensity, with a red-shift in λ_{max} (CD signal position), suggesting extended and more stable *P*-helical assembly as opposed to the initially formed *M*-helical assembly in pure HFIP (Figure 2c). CD studies of NCDP **1** performed in DMSO alone and in HFIP containing co-solvents not isostructural with DMSO under similar conditions did not show any chiroptical switching properties (Figures S1 and S6 in the Supporting Information). Thus, DMSO in HFIP is responsible for the observed *M*- to *P*-helical inversion in the chiral supramolecular assembly of NCDP **1**. We also carried out CD measurements on NCDP **1** at 50 μM in both HFIP and DMSO/HFIP (15:85, v/v) using 10 mm path length cuvettes to rule out any absence of CD signals at low concentrations due to insufficient sensitivity when 1 mm path length cuvettes were

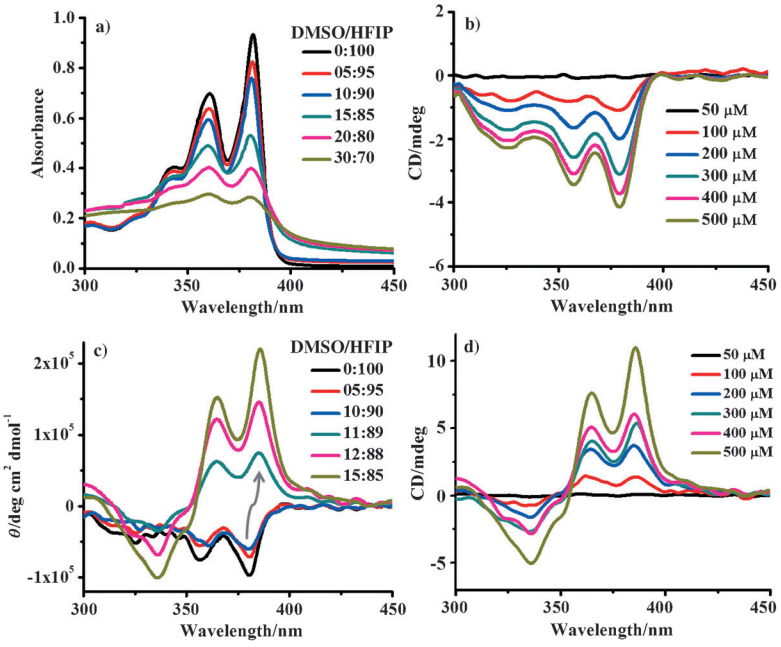

Figure 2. a) UV/Vis absorption spectra of NCDP **1** (100 μM) in HFIP with increasing volume fractions of DMSO under ambient conditions, b) CD spectra of NCDP **1** in HFIP at increasing concentrations from 50 μM to 500 μM, c) CD spectra of NCDP **1** (500 μM) in HFIP with increasing volume fractions of DMSO, d) CD spectra of NCDP **1** in DMSO/HFIP (15:85, v/v) at concentrations from 50 μM to 500 μM; DMSO: dimethyl sulfoxide; HFIP: 1,1,1,3,3,3-hexafluoropropan-2-ol. Arrow in c) indicates the chiroptical switching from *M*- to *P*-helical assembly.

used. This CD study using 10 mm path length cuvettes did not show any noteworthy additional signals, emphasizing the significance of the minimum monomer concentration required for aggregation of NCDP **1** (Figure S5 in the Supporting Information). To rule out linear dichroism (LD)-induced artefacts in the observed helical assembly and chiroptical switching properties of NCDP **1**, LD spectra were recorded under similar experimental conditions and showed no significant signals (Figure S8 in the Supporting Information). The observed chiroptical switching from monosignate *M*-helical (in HFIP) to bisignate *P*-helical handedness in the NCDP **1** assembly may be attributed to strong excitonic interactions and preferential helical stabilization of this system in DMSO/HFIP (15:85, v/v). It is proposed that the DMSO molecules locally reorganize the HFIP solvent clusters around the NCDP. The methyl groups ($-CH_3$) of DMSO can preferentially solvate NCDP **1** to induce a hydrophobic effect, which subsequently drives the inversion of the *M*-helical to the thermodynamically more stable *P*-helical assembly of NCDP **1** in DMSO/HFIP. Concentration-dependent CD spectra were recorded in DMSO/HFIP (15:85, v/v) to study the effect of monomer concentration on the observed chiroptical switching of the helical assembly of NCDP **1**. The CD spectra of NCDP **1** from 100 to 500 μM in DMSO/HFIP (15:85, v/v) showed a bisignate positive Cotton signal (*P*-helical bias) regardless of the concentration (Figure 2d). This further emphasized the crucial role of the DMSO/HFIP (15:85, v/v) solvent composition in stabilizing the thermodynamically more stable *P*-helical assembly of NCDP **1**. Next, variable-temperature CD studies were carried out to probe the effect of temperature on the chiroptical switching and stability of the *P*-helical assembly. CD spectra recorded for NCDP **1** (500 μM) in DMSO/HFIP (15:85, v/v) between 25 and 60 °C showed no significant changes in the sign or intensity of the CD signal during the heating and cooling cycles. Thus, variable-temperature CD study ruled out any influence of temperature on the observed chiroptical switching and asserted the stability of chiral aggregates at higher temperatures (data not shown). The stability of *P*-helical aggregates of NCDP **1** can be attributed to strong intermolecular aromatic π–π interactions between the NDI cores supported by N−H···O hydrogen bonding between peripheral CDP auxiliaries.

Dynamic light-scattering (DLS) studies were carried out to obtain direct evidence for the self-assembly of NCDP **1** in solution. DLS data for NCDP **1** at 500 μM in solution showed the presence of aggregates, and the aggregate size was found to vary with solvent composition (Figure 3). The hydrodynamic sizes of the aggregates of NCDP **1** were found to be 37 nm in HFIP, and 210, 269, and 531 nm in 5% DMSO, 11% DMSO, and 15% DMSO in HFIP, respectively. Furthermore, the observed chirality could be unequivocally attributed to self-assembled NCDP **1** (500 μM) aggregates in solution by recording CD spectra in DMSO/HFIP (15:85, v/v) before and after centrifugation and filtration of the solution through a 0.45 μm filter. The CD spectrum recorded from the as-prepared sample showed a strong bisignate CD signal, whereas the filtered solution did not show any CD signal, as the centrifugation and filtration process had removed the chiral aggregates (Figure S7 in the Supporting Information). This study corroborated the observed chirality and its origin through intermolecular self-assembly of monomeric NCDP supramolecular synthons in solution.

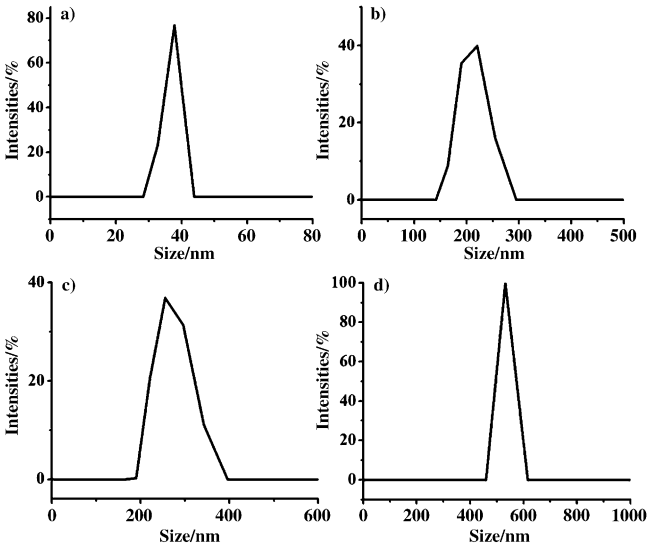

Figure 3. Dynamic light-scattering (DLS) studies of NCDP **1** at 500 μM (self-assembled chiral aggregates) in a) HFIP (37 nm), b) 5% DMSO in HFIP (210 nm), c) 11% DMSO in HFIP (269 nm), and d) 15% DMSO in HFIP (531 nm). Observed hydrodynamic size distributions are given in parentheses.

Quantum chemical calculations were carried out to further understand the magnitude of intermolecular interactions in all of the NCDP molecules (**1**–**6**) in their *M*- and *P*-helical supramolecular assembly states. Four dimer models were constructed for the *P*- and *M*-helices for NCDPs **1**–**6** from their respective monomers. The differences between the respective models lie in the conformational arrangement of the monomer units. Since these molecules have long linear side chains, several conformations are possible, of which four straightforward possibilities were considered. The interaction energies for all the models of the NCDP **1** molecule were calculated at the semiempirical PM7 and density functional M06/6-31+G* levels of theory. The results obtained at these two levels of theory were in reasonable agreement with each other (Table 1). The semiempirical PM7 method has been shown to reasonably capture nonbonded interactions involving both electrostatic and dispersion interactions.[28] The interaction energies for NCDP **2** were also calculated at both the PM7 and M06 levels, and were again found to be mutually consistent (data not shown). Based on this, the other molecules were modelled at the computationally less expensive PM7 level of theory. The optimized geometries of the most stable *M*- and *P*-helical dimers for NCDP **1** are depicted in Figure 4. Molecular models for the *P*- and *M*-helical supramolecular motifs for NCDP **1** are shown in Figure 1. The interaction energies corresponding to the formation of such dimers were found to

Table 1. Relative energies (kcal mol^{-1}) of the *P*- and *M*-helical models of NCDP **1** dimers along with the interaction energies calculated at the PM7 (I_a) and M06/6-31+G* (I_b) levels of theory.[a]

Model	Relative energy	Interaction energy (I_a)	Interaction energy (I_b)
I-*P*	0.0 (0.0)	−67.4	−63.4
II-*P*	15.5 (17.6)	−52.0	−45.8
III-*P*	25.9 (41.8)	−41.5	−21.6
IV-*P*	32.0 (42.4)	−35.4	−21.1
I-*M*	12.7 (25.2)	−54.7	−38.2
II-*M*	18.3 (33.3)	−49.2	−30.2
III-*M*	32.5 (45.3)	−35.0	−18.1
IV-*M*	40.3 (54.2)	−27.2	−9.3

[a] Relative energy values in parentheses correspond to calculations carried out at the M06/6-31+G* level. I_a: Interaction energies calculated using the energies of the optimized dimers and those of the optimized monomer at the PM7 level. I_b: Interaction energies calculated using the single-point energy of the optimized dimers and the single-point energy of the optimized monomer at the M06/6-31+G* level (optimization at the PM7 level). I to IV represent the dimers formed from four different conformations considered for NCDP **1** (see Computational Details section) in *P*- (right-handed) and *M*- (left-handed) helical arrangements, respectively.

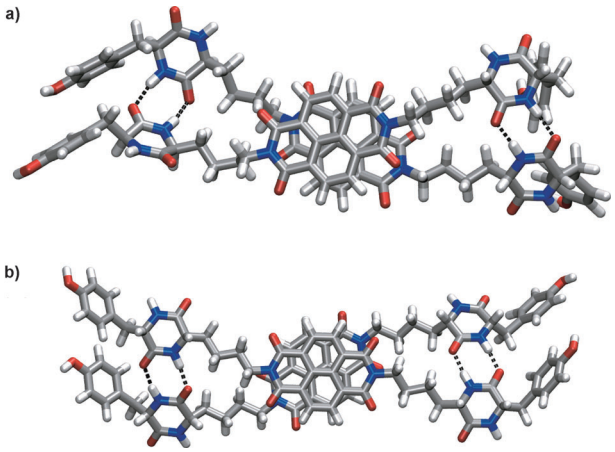

Figure 4. Optimized structures of a) *P*-helical dimer (**I-*P***) and b) *M*-helical dimer (**I-*M***) of NCDP **1**.

be more favourable for the *P*-helices compared to the *M*-helices. Interestingly, the CD intensity of a *P*-helix at a given concentration of NCDP **1** in DMSO/HFIP was found to be higher than that of an *M*-helix of NCDP **1** in HFIP, indicating a higher stability of the former. Both the *P*- and *M*-helices of NCDP **1** dimer involve hydrogen-bonding interactions between the CDP amide groups. The hydroxyl groups of the tyrosine moieties in NCDP **1** are unlikely to form hydrogen bonds between them as the distance between the oxygen atoms of the two monomer units is about 4 Å. It should be noted that the *P*-helical models were found to be thermodynamically more stable than the *M*-helical assemblies. The stacking energy for the basic naphthalenediimide stacked dimers was calculated to be 20 kcal mol^{-1} at the M06/6-31+G* level of theory. Comparison of the interaction energies given in Table 1 indicates that the hydrogen-bonding interactions significantly contribute to the overall stability of the supramolecular assembly. The intermolecular hydrogen bonding between the amide groups of the constituent monomers of the corresponding dimers was also verified by calculating second-order perturbative interaction energies by means of natural bond orbital (NBO) analysis at the ab initio HF level using the 6-31+G* basis set. The interaction energies of the four amide groups are given in Table S7 (see the Supporting Information). From the data, it can be noted that there is strong intermolecular hydrogen bonding between the amide groups of the monomers. Explicit calculations involving the solvent molecules are not practical to examine the role of the solvent in the *M*- to *P*-helical transition.

However, based on the computational results and experimental observations, possible determinants of the chiroptical switching may be proposed, as discussed below. The twist angles (helical twist between the two monomer units) calculated for the helical models were found to range between 35 and 40°. The hydrogen bond distances between the amide groups at either side of the monomer units were found to lie in the range 1.75–1.95 Å. *P*- and *M*-helical models of the supramolecular assembly consisting of 24 monomer units are presented in Figure 1. In these models, 12 monomers per turn were included, with a distance of 3 Å between any two adjacent molecules.

Next, we probed the effect of the α-substituent (R = $-CH_2C_6H_5$, $-CH_2CH(CH_3)_2$, −H) in the CDP auxiliary on the assembly properties of NCDPs. UV/Vis absorption studies of NCDPs **2**–**4** revealed aggregation characteristics similar to those of NCDP **1**. With increasing volume fraction of DMSO in HFIP, NCDPs **2**–**4** (100 μM) showed decreases in absorbance and hypsochromic shifts in the region 300–400 nm (Figures S9 and S10(a) in the Supporting Information). NCDPs **2** and **3** (500 μM) showed monosignate negative CD signals in the region 300–400 nm in pure HFIP (*M*-helical assembly). Similarly to NCDP **1**, NCDPs **2** and **3** both showed chiroptical switching from a monosignate *M*-helical Cotton signal to a bisignate *P*-helical Cotton signal on increasing the volume fraction of DMSO in HFIP (Figure 5). Notably, the solvent compositions (DMSO/HFIP, v/v) giving the maximum positive Cotton signals were specifically different for NCDPs **1**–**3** (15:85, 30:70, and 40:60, respectively) (Figure 2c, Figure 5). This variation in the solvent composition of DMSO/HFIP may be necessary to attain balanced polarity, hydrophobicity, and hydrogen-bonding interactions to trigger chiroptical switching from *M*- to *P*-helical assemblies of NCDPs **1**–**3** with different α-substituents. In general, these results suggest that the chiral assembly and chiroptical switching of NCDPs **1**–**3** is independent of the nature of the bulky α-substituent (R) on the second amino acid in the CDP auxiliary.

The remarkable chiroptical switching phenomenon further encouraged us to investigate the effect of the chirality of the second amino acid in the CDP auxiliaries. Initially, we examined the effect of an achiral amino acid (Gly) on the chiral assembly and solvent-dependent chiroptical switching property. NCDP **4** with cyclo(L-Lys-Gly) served as an effec-

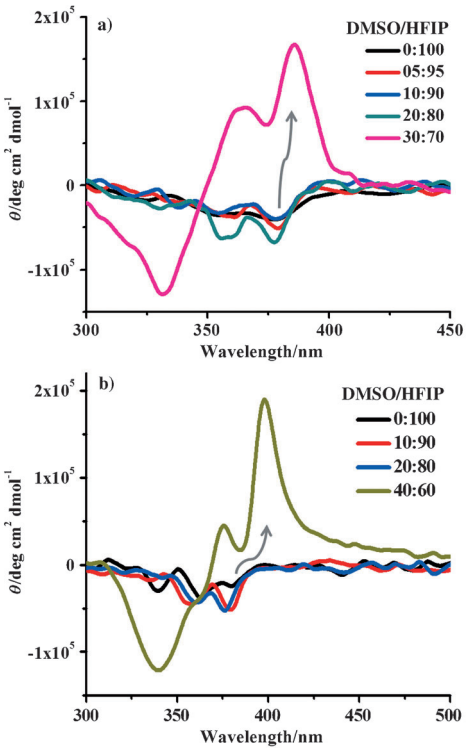

Figure 5. CD spectra of a) NCDP **2** and b) NCDP **3** in HFIP with increasing volume fractions of DMSO at 500 μM. Grey arrows indicate the chiroptical switching from *M*- to *P*-helical assemblies.

tive control to study the transfer of chiral information from a distant chiral centre on L-lysine to the NDI core as well as to understand the influence of the second chiral centre on the observed assembly properties of NCDPs **1**–**3**. In contrast to all the other NCDPs studied, NCDP **4** exhibited mirror-image fluorescence emission in the region 380–450 nm in HFIP (Figure S10(b) in the Supporting Information). The monomeric emission band (380–450 nm) of NCDP **4** decreased with increasing volume fraction of DMSO in HFIP and subsequently a new emission band at around 540 nm was observed due to excimer-like aggregation.[24a] At a solvent composition of DMSO/HFIP (20:80, v/v), complete quenching of the monomeric emission band was observed, accompanied by a colour change of the solution from violet (monomeric emission) to yellow (excimer-like emission) under UV light. To study the intermolecular hydrogen bonding (CDP auxiliary) in NCDP **4**, variable-temperature ^{1}H NMR spectra were recorded. NCDP **4** showed upfield shifts of the CDP amide signals at $\delta = 8.18$ and 7.98 ppm to $\delta = 7.91$ and 7.72 ppm, respectively, on increasing the temperature from 25 to 80 °C, which confirmed the hydrogen-bonding network in its assembled structure (Figure S11 in the Supporting Information). Similar upfield shifts of the amide signals from $\delta = 8.05$ and 8.01 ppm to $\delta = 7.78$ and 7.67 ppm on increasing the temperature from 25 to 80 °C were observed for NCDP **1** (Figure S12 in the Supporting Information). Concentration-dependent ^{1}H NMR spectra of NCDP **1** in [D_6]DMSO revealed the presence of strong intermolecular π–π stacking of the NDI chromophores and hydrogen-bonding between the CDP units of NCDP, as evidenced by a downfield shift of the CDP amide proton signals accompanied by an upfield shift of the NDI chromophore proton signals with increasing concentration (Figure S13 in the Supporting Information).[29]

Surprisingly, flat CD signals were observed for NCDP **4** at all possible concentrations and solvent combinations of DMSO/HFIP, indicating an absence of chiral bias or switching property in its supramolecular assembly (Figure S14 in the Supporting Information). The absence of chiral bias and chiroptical switching in NCDP **4** may be attributed to the perfectly symmetrical nature of the resultant assembly. The absence of a bulky α-substituent (R) and the chiral centre on the second amino acid of the CDP auxiliary lead to insignificant interconversion energy between the *M*- and *P*-helical assemblies. These results clearly emphasize the crucial role of the chiral centre as well as the bulky α-substituent on the second amino acid of the CDP auxiliary with regard to the solvent-induced preferential helical bias and chiroptical switching behaviour of NCDP supramolecular assemblies.

The origins of this distinct behaviour of NCPD **4** compared to the other three NCDPs (**1**–**3**) discussed above were examined by further quantum chemical calculations. The average interaction energies for the four *P*- and *M*-type helical dimer models of the six NCDP molecules are represented in Figure 6. From the data, it is observed that for NCDPs

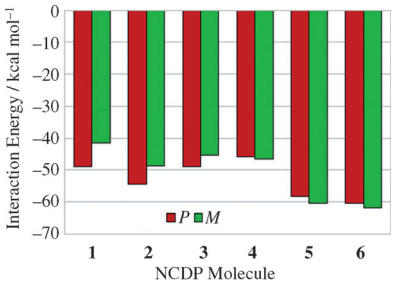

Figure 6. Average interaction energies for the *P*- and *M*-helical dimers for all six molecules (NCDPs **1**–**6**) calculated at the PM7 level of theory.

2 and **3**, the *P*-helical dimer is thermodynamically more stable than the *M*-helical dimer as in the case of NCDP **1**. The structures of the most stable *P*- and *M*-helical dimers at the PM7 level of theory, along with the hydrogen bonds between the amide groups, are depicted in Figure S17 (see the Supporting Information). The twist angles and the hydrogen-bonding distances between the cyclic dipeptide moieties calculated for the other models were found to be similar to those obtained for NCDP **1**. Interaction energy calculations on the dimers of NCDP **4** indicated comparable stabilities for both the *P*- and *M*-forms (Figure 6). Visual inspection of the modelled structures indicates that the *P*- and *M*-forms of the supramolecular assembly of NCDP **4** are very similar (Figure S17). Hence, molecules of NCDP **4** are likely to be

arranged almost equally in both forms, resulting in no CD signal, as observed experimentally. The interaction energies for all eight models for NCDPs **2**, **3**, and **4** are given in detail in Tables S1–S6 (see the Supporting Information). The intermolecular hydrogen-bonding interaction energies for the most stable dimers of the above molecules are given in Table S7 (see the Supporting Information).

We further investigated the effect of a change in chirality of the second amino acid in the CDP auxiliary on the solvent-dependent chiral assembly and chiroptical switching of the NCDP aggregates. NCDPs **5** and **6** (epimers of NCDP **1** and **2**) with D-Tyr and D-Phe, respectively, at 100 μM exhibited a decrease in the absorbance intensity and a slight hypsochromic shift with increasing volume fraction (v/v) of DMSO in HFIP due to solvent-induced aggregation (Figure S15 in the Supporting Information). The CD spectra of NCDPs **5** and **6** at 500 μM in HFIP showed flat CD signals in the region 300–400 nm, indicating no specific helical bias in their molecular assemblies. NCDPs **5** and **6** did not show any significant spectral changes upon increasing the volume fraction of DMSO (v/v) in HFIP, except that the flat CD signals in HFIP gradually became weak negative CD signals (Figure S16 in the Supporting Information). The average interaction energies for NCDPs **5** and **6** are given in Figure 6, from which it is apparent that the *M*-helical dimer was marginally more stable than the *P*-helical dimer in both cases. The helical angles and hydrogen-bonding distances were in similar ranges to those of the other molecules. Energy-minimized models for the *M*- and *P*-helical dimers of NCDPs **5** and **6** are given in Figure S17. Intermolecular hydrogen-bonding interaction energies for the amides of the two monomers (Table S7) are indicative of strong bonding between them, leading to dimers, in addition to π-stacking interactions. NCDPs **5** and **6** with D-amino acids in the second positions of their CDP auxiliaries did not display significant CD signals due to mismatched chiral centres on the two amino acids of the CDP auxiliary, resulting in irregular aggregation. Thus, NCDPs **4**–**6** with no significant CD features in HFIP did not exhibit chiroptical switching in the mixed solvent (DMSO/HFIP). This confirmed that the α-substituent (R) and the chirality of the amino acid play essential roles in the solvent-induced helical chirality and chiroptical switching of the supramolecular assemblies of the NCDPs. Therefore, the observed chiral aggregation of NCDPs **1**–**3** in HFIP is due to the clustering and stabilization of *M*-type helical assemblies, which is influenced by the α-substituent and the chirality (L) of the amino acids in the CDP auxiliary. The chiroptical switching behaviour of NCDPs **1**–**3** in DMSO/HFIP can be attributed to an effective local contribution of DMSO through the hydrophobic effect of its methyl groups and possible hydrogen bonding as an acceptor in reorganizing the HFIP clusters around the NCDP assembly, among other bulk effects of the mixed solvent.[30]

Next, we investigated the reversibility of the chiroptical switching property of NCDP **1** between *M*- and *P*-type helical assemblies by carrying out CD studies in HFIP and DMSO/HFIP (15:85, v/v) in cycles. Specifically, the CD spectrum of NCDP **1** (500 μM in HFIP) was recorded and the solvent was removed in vacuo. The residue was redissolved in DMSO/HFIP (15:85, v/v) and the CD spectrum was recorded to complete the first cycle. For the next cycle, the mixed solvent (DMSO/HFIP) was removed in vacuo, the residue was redissolved in HFIP, and the CD spectrum was recorded. This procedure was followed over further cycles and the full data is shown in Figure 7a. This study

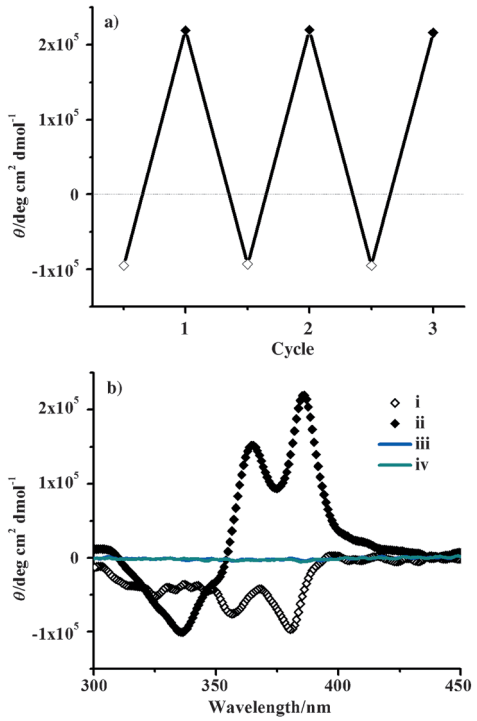

Figure 7. Solution and drop-cast thin-film CD spectra of NCDP **1**. a) CD intensity plotted against each cycle of study for NCDP **1** at 500 μM in HFIP (◇ $\lambda = 380$ nm) and DMSO/HFIP (15:85, v/v; ◆ $\lambda = 385$ nm), b) CD spectra of NCDP **1** at 500 μM in solution (i: HFIP, ii: DMSO/HFIP (15:85, v/v)) and drop-cast thin films (iii: from HFIP, iv: from DMSO/HFIP (15:85, v/v)).

clearly demonstrated the reversibility of the solvent-induced chiroptical switching, as reflected by the retention of the CD features for NCDP **1** in HFIP (*M*-helicity) and DMSO/HFIP (*P*-helicity) even after three cycles of solvent removal and redissolution (Figure 7a). In addition, CD spectra were recorded from thin films of NCDP **1** to further confirm the observed solvent-induced reversible chiroptical switching. Thin films were prepared by drop-casting NCDP **1** from solutions in HFIP and DMSO/HFIP (15:85, v/v) onto quartz substrates. The CD spectra of the thin films showed flat signals indicating no chiral bias in the solid state, which further emphasized the crucial role of the solvent in the helical assembly and reversible chiroptical switching of the NCDPs (Figure 7b).

The intriguing solvent (DMSO/HFIP)-induced chiroptical switching of self-assembled chiral aggregates of NCDPs prompted us to further generalize this effect in other solvent

systems. Addition of solvents such as chloroform, dichloromethane, or 1-methyl-2-pyrrolidone failed to induce chiroptical switching of the *M*-helical aggregates of NCDP **1** in HFIP. Next, we examined isostructural (ketone and alcohol) solvents such as acetone, 2-pentanone, 3-pentanone, cyclopentanone, and cyclohexanone, as they possess variable linear or cyclic alkyl substituents on the C=O functionality (Table 2), as well as 2-propanol (isopropanol). The CD spectra of NCDP **1** (500 μM) in HFIP with varying volume fractions of the above mentioned solvents were recorded. Remarkably, all of these solvents showed chiroptical switching similar to that seen in the DMSO/HFIP system (Figures S2–S4 in the Supporting Information). Interestingly, the volume fractions required to obtain the maximum positive Cotton signal upon chiral inversion varied with each solvent combination (25% acetone, 25% 2-pentanone, 25% 3-pentanone, 25% cyclopentanone, 30% cyclohexanone, and 35% isopropanol in HFIP). These results also revealed that the solvent composition required to induce the maximum chiral inversion was the same for all of the ketones (except cyclohexanone), that is, 25% in HFIP. Notably, isopropanol, the non-fluorinated isostructural analogue of HFIP, exhibited a completely opposite effect by inducing chiroptical switching of the *M*-helical assembly of NCDP **1** in HFIP to the thermodynamically more stable *P*-helical assembly. This result may have broader implications in understanding the distinct role of fluorinated solvents compared to their non-fluorinated analogues. Overall, the above CD data are in agreement with the changes observed for NCDP **1** in DMSO/HFIP and show the generality of the chiroptical switching phenomena in HFIP containing solvents isostructural to DMSO (Figures S2–S4).

Table 2. Molecular structures of various solvents that induce chiral switching of *M*-helical aggregates of NCDP **1** (500 μM) in HFIP and % volume fractions of each solvent in HFIP to achieve maximum positive Cotton signal upon chiral inversion.

Solvent	Solvent structure	% Volume fraction of co-solvent in HFIP (at maximum inversion)
dimethyl sulfoxide		15
acetone		25
2-pentanone		25
3-pentanone		25
cyclopentanone		25
cyclohexanone		30
isopropanol		35

Though the *P*-helical dimer was found to be thermodynamically more stable in the case of NCDPs **1**–**3**, *M*-helical supramolecular complexes were observed in the CD spectroscopic studies in HFIP. However, with gradual addition of DMSO, the *P*-helical complexes were formed. It is proposed that hydrogen-bond dynamics and hydrophobic effects within the supramolecular complex and with the solvent play major roles in this chiral reversal. Based on quantum chemical/DFT calculations and spectroscopic studies, it has been proposed that the helix-stabilizing effect of specific compositions of HFIP in peptides can be attributed to a clustering and coating effect, entropic and enthalpic factors, and variations in the kinetics of conformational changes.[26] It is reasonable to postulate that similar effects are operative in the initial stabilization of the *M*-helical assemblies of NCDPs **1**–**3**. It is possible that the amide groups (both C=O and N–H) of NCDP in the less stable *M*-helix may form intermolecular hydrogen bonds, both with each other and with the solvent cluster. In such a scenario, the energy difference between the *M*- and *P*-helices will be compensated by the hydrogen bonding with the solvent, as well as by entropic and enthalpic factors. In the mixed solvent, the DMSO molecules reorganize the solvent cluster of HFIP through hydrogen bonding and localized hydrophobic effects, which drive the switching from the initial *M*-type to the thermodynamically more stable *P*-type helical assembly. Chiral reversal is not observed in **5** and **6** since the energy differences between the two states are calculated to be not so significant (Figure 6). In these two cases, the marginally more stable *M*-helical form is observed experimentally. Recently, Faul et al.[4f] showed a similar effect in a symmetrical sugar-based perylenediimide derivative, whereby a *P*-helical model was thermodynamically more stable than the *M*-helix.

Conclusion

In summary, symmetrical naphthalenediimides with CDP chiral auxiliaries (NCDPs) have been designed and studied to orchestrate preferential supramolecular helical assembly. The contributions of intermolecular aromatic π-stacking and hydrogen-bonding interactions have been established by various experimental studies and quantum chemical calculations. The solvent-dependent helical supramolecular assembly and chiroptical switching (*M*- to *P*-type) of NCDP assemblies have been validated through a series of concentration-, solvent-, and temperature-dependent CD studies. NCDPs **1**–**3** formed *M*-helical assemblies in HFIP, which underwent chiral inversion to form thermodynamically more stable *P*-helical assemblies in DMSO/HFIP mixtures. Further CD studies revealed the significance of the α-substituent and the corresponding chirality of the peripheral amino acid in the CDP auxiliary with regard to solvent-induced helical assembly and the chiroptical switching properties of the NCDPs. The characteristic chiroptical switching of the helical assembly of NCDP is reversible and the system can be reversibly transformed between *M*- and *P*-helices by cycles of solvent removal and redissolution. Overall, the remarkable helical assembly characteristics of the NCDPs reported herein demonstrate the crucial role of the CDP chiral auxiliary. We hope that the present study might in-

spire the development of novel chiral auxiliaries to master the art of preferential helical assembly of designed supramolecular synthons so as to obtain smart self-assembled systems and materials, as well as for chiroptical applications. Further studies aimed at probing the roles of external stimuli in controlling the chiral molecular self-assembly are underway in our laboratory.

Experimental Section

General: Amino acids and coupling reagents were obtained from Novabiochem; other chemicals, solvents, and analytical grade reagents were obtained from Sigma–Aldrich and were used as purchased without any further purification. Elemental analysis was carried out on a Thermo Scientific FLASH 2000 organic element analyzer. ^{1}H and ^{13}C NMR spectra were acquired on a Bruker AV-400 spectrometer with chemical shifts reported in parts per million (in $CDCl_3$/[D_6]DMSO/D_2O, with tetramethylsilane as internal standard). Mass spectra were obtained on a Bruker Ultraflex II MALDI-TOF spectrometer. UV/Vis spectra and fluorescence spectra were recorded on a Perkin–Elmer Lambda 900 spectrophotometer and a Perkin–Elmer LS 55 spectrophotometer, respectively, using 1 mm quartz cuvettes at ambient temperature. Solution and thin-film circular dichroism (CD) and linear dichroism (LD) measurements were performed on a JASCO J-815 spectropolarimeter under N_2 atmosphere using 1 mm path length quartz cuvettes unless otherwise mentioned and the values are quoted in molar ellipticity, θ (deg cm^2 dmol^{-1}). Dynamic light-scattering (DLS) measurements were carried out on a NanoZS analyser (Malvern, UK) under ambient conditions.

Computational details: The monomers for all six models under study (NCDPs **1**–**6**) were modelled using the GaussView 05 program.[31] The *P*- and *M*-helical dimers were modelled from the initial monomer structure. The *P*-helical dimers were modelled by placing the second monomer at a distance of 3 Å from the first monomer and then rotating the second monomer in the anticlockwise direction by 30°. The twist angle of 30° was chosen on the basis of the M06/6–31+G* optimization of the dimer of naphthalenediimide. Similarly, the *M*-helical dimer was also modelled in the same way by rotating the second monomer in the clockwise direction. The monomer and the two resultant dimers were then optimized at the PM7 level of theory using the MOPAC 2012 program.[32] Based on test calculations, we considered up to four different conformations for each molecule under study. Furthermore, the optimized monomer and the dimers of NCDPs **1** and **2** were further subjected to single-point energy calculations at the M06 level[33] of theory using the 6–31+G* basis set and the Gaussian 09 program.[34] The interaction energies were calculated as the differences between the energies of the dimers and the monomers. The donor–acceptor interactions between the individual monomers resulting in the formation of the dimers were analysed for all of the NCDP molecules under study using natural bond orbital (NBO) analysis carried out at the ab initio HF level of theory using the 6–31+G* basis set. The NBO analysis was carried out using the NBO program 3.1[35] included in the G09 suite of programs.

Acknowledgements

We thank Prof. C. N. R. Rao, FRS for constant support, JNCASR, Department of Biotechnology (DBT)-Innovative Young Biotechnologist Award (IYBA) and the Department of Science and Technology (DST), India, for financial support. We also thank the CSIR, New Delhi, for awarding a senior research fellowship to SM and the DST for awarding an Inspire fellowship to VP.

[1] a) J. D. Watson, F. H. C. Crick, *Nature* **1953**, *171*, 737–738; b) L. Pauling, R. B. Corey, H. R. Branson, *Proc. Natl. Acad. Sci. USA* **1951**, *37*, 205–211; c) J. E. Hein, D. G. Blackmond, *Acc. Chem. Res.* **2012**, *45*, 2045–2054.

[2] a) E. Yashima, K. Maeda, H. Iida, Y. Furusho, K. Nagai, *Chem. Rev.* **2009**, *109*, 6102–6211; b) B. L. Feringa, R. A. van Delden, N. Koumura, E. M. Geertsema, *Chem. Rev.* **2000**, *100*, 1789–1816; c) J. W. Canary, *Chem. Soc. Rev.* **2009**, *38*, 747–756.

[3] a) A. E. Rowan, R. J. M. Nolte, *Angew. Chem.* **1998**, *110*, 65–71; *Angew. Chem. Int. Ed.* **1998**, *37*, 63–68; b) J. L. Serrano, T. Sierra, *Coord. Chem. Rev.* **2003**, *242*, 73–85; c) M. A. Mateos-Timoneda, M. Crego-Calama, D. N. Reinhoudt, *Chem. Soc. Rev.* **2004**, *33*, 363–372; d) Y. Wang, J. Xu, Y. Wang, H. Chen, *Chem. Soc. Rev.* **2013**, *42*, 2930–2962.

[4] a) H. Engelkamp, S. Middelbeek, R. J. M. Nolte, *Science* **1999**, *284*, 785–788; b) H. Nakashima, M. Fujiki, J. R. Koe, M. Motonaga, *J. Am. Chem. Soc.* **2001**, *123*, 1963–1969; c) A. Brizard, C. Aimé, T. Labrot, I. Huc, D. Berthier, F. Artzner, B. Desbat, R. Oda, *J. Am. Chem. Soc.* **2007**, *129*, 3754–3762; d) J. Cui, A. Liu, Y. Guan, J. Zhang, Z. Shen, X. Wan, *Langmuir* **2010**, *26*, 3615–3622; e) Y. W. Huang, J. C. Hu, W. F. Kuang, Z. X. Wei, C. F. J. Faul, *Chem. Commun.* **2011**, *47*, 5554–5556; f) J. C. Hu, W. F. Kuang, K. Deng, W. J. Zou, Y. W. Huang, Z. X. Wei, C. F. J. Faul, *Adv. Funct. Mater.* **2012**, *22*, 4149–4158.

[5] a) M. Fujiki, *J. Am. Chem. Soc.* **2000**, *122*, 3336–3343; b) M. Fujiki, J. R. Koe, M. Motonaga, H. Nakashima, K. Terao, A. Teramato, *J. Am. Chem. Soc.* **2001**, *123*, 6253–6261; c) A. P. H. J. Schenning, M. Fransen, E. W. Meijer, *Macromol. Rapid Commun.* **2002**, *23*, 265–270.

[6] S. Mayer, G. Maxein, R. Zentel, *Macromolecules* **1998**, *31*, 8522–8525.

[7] a) M. M. Green, C. Khatri, N. C. Peterson, *J. Am. Chem. Soc.* **1993**, *115*, 4941–4942; b) E. Yashima, K. Maeda, O. Sato, *J. Am. Chem. Soc.* **2001**, *123*, 8159–8160; c) K. Sakajiri, T. Sugisaki, K. Moriya, S. Kutsumizu, *Org. Biomol. Chem.* **2009**, *7*, 3757–3762.

[8] a) H. Goto, E. Yashima, Y. Okamoto, *Chirality* **2000**, *12*, 396–399; b) T. Yamada, Y. Nagata, M. Suginome, *Chem. Commun.* **2010**, *46*, 4914–4916; c) Y. Nagata, T. Nishikawa, M. Suginome, *Chem. Commun.* **2012**, *48*, 11193–11195; d) T. Qi, V. Maurizot, H. Noguchi, T. Charoenraks, B. Kauffmann, M. Takafuji, H. Ihara, I. Huc, *Chem. Commun.* **2012**, *48*, 6337–6339.

[9] A. Lohr, M. Lysetska, F. Würthner, *Angew. Chem.* **2005**, *117*, 5199–5202; *Angew. Chem. Int. Ed.* **2005**, *44*, 5071–5074.

[10] K. Jyothish, M. Hariharan, D. Ramaiah, *Chem. Eur. J.* **2007**, *13*, 5944–5951.

[11] S. Cantekin, Y. Nakano, J. C. Everts, P. van der Schoot, E. W. Meijer, A. R. A. Palmans, *Chem. Commun.* **2012**, *48*, 3803–3805.

[12] a) V. M. Guelev, M. T. Harting, R. S. Lokey, B. L. Iverson, *Chem. Biol.* **2000**, *7*, 1–8; b) S. Guha, S. Saha, *J. Am. Chem. Soc.* **2010**, *132*, 17674–17677; c) G. G. Holman, M. Zewail-Foote, A. R. Smith, K. A. Johnson, B. L. Iverson, *Nat. Chem.* **2011**, *3*, 875–881; d) G. W. Collie, R. Promontorio, S. M. Hampel, M. Micco, S. Neidle, G. N. Parkinson, *J. Am. Chem. Soc.* **2012**, *134*, 2723–2731; e) M. B. Avinash, T. Govindaraju, *Adv. Funct. Mater.* **2011**, *21*, 3875–3882.

[13] a) S. Alp, S. Erten, C. Karapire, B. Koz, A. O. Doroshenko, S. Icli, *J. Photochem. Photobiol. A* **2000**, *135*, 103–110; b) B. Erten, Y. Posokhov, S. Alp, S. Icli, *Dyes Pigm.* **2005**, *64*, 171–178.

[14] a) P. Pengo, G. D. Pantos, S. Otto, J. K. M. Sanders, *J. Org. Chem.* **2006**, *71*, 7063–7066; b) H. Shao, J. Seifert, N. C. Romano, M. Gao, J. J. Helmus, C. P. Jaroniec, D. A. Modarelli, J. R. Parquette, *Angew. Chem.* **2010**, *122*, 7854–7857; *Angew. Chem. Int. Ed.* **2010**, *49*, 7688–7691.

[15] a) H. Shao, T. Nguyen, N. C. Romano, D. A. Modarelli, J. R. Parquette, *J. Am. Chem. Soc.* **2009**, *131*, 16374–16376; b) H. Shao, J. R. Parquette, *Chem. Commun.* **2010**, *46*, 4285–4287; c) H. Shao, M. Gao, S. H. Kim, C. P. Jaroniec, J. R. Parquette, *Chem. Eur. J.* **2011**, *17*, 12882–12885.

[16] W. S. Horne, N. Ashkenasy, M. R. Ghadiri, *Chem. Eur. J.* **2005**, *11*, 1137–1144.
[17] a) T. D. M. Bell, S. Yap, C. H. Jani, S. V. Bhosale, J. Hofkens, F. C. De Schryver, S. J. Langford, K. P. Ghiggino, *Chem. Asian J.* **2009**, *4*, 1542–1550; b) M. M. Durban, P. D. Kazarinoff, C. K. Luscombe, *Macromolecules* **2010**, *43*, 6348–6352.
[18] a) M. R. Molla, A. Das, S. Ghosh, *Chem. Commun.* **2011**, *47*, 8934–8936; b) M. R. Molla, S. Ghosh, *Chem. Eur. J.* **2012**, *18*, 1290–1294.
[19] M. B. Avinash, T. Govindaraju, *Adv. Mater.* **2012**, *24*, 3905–3922.
[20] a) M. B. Avinash, T. Govindaraju, *Nanoscale* **2011**, *3*, 2536–2543; b) M. B. Avinash, E. Verheggen, C. Schmuck, T. Govindaraju, *Angew. Chem.* **2012**, *124*, 10470–10474; *Angew. Chem. Int. Ed.* **2012**, *51*, 10324–10328; c) M. B. Avinash, T. Govindaraju, *J. Phys. Chem. Lett.* **2013**, *4*, 583–588.
[21] M. Pandeeswar, M. B. Avinash, T. Govindaraju, *Chem. Eur. J.* **2012**, *18*, 4818–4822.
[22] a) J. C. MacDonald, G. M. Whitesides, *Chem. Rev.* **1994**, *94*, 2383–2420; b) C. Prasad, *Peptides* **1995**, *16*, 151–164; c) K. R. C. Prakash, Y. Tang, A. P. Kozikowski, J. L. Flippen-Anderson, S. M. Knoblach, A. I. Faden, *Bioorg. Med. Chem.* **2002**, *10*, 3043–3048; d) M. B. Martins, I. Carvalho, *Tetrahedron* **2007**, *63*, 9923–9932.
[23] a) K. Hanabusa, Y. Matsumoto, T. Miki, T. Koyama, H. Shirai, *J. Chem. Soc. Chem. Commun.* **1994**, 1401–1402; b) R. J. Bergeron, O. Phanstiel, G. W. Yao, S. Milstein, W. R. Weimar, *J. Am. Chem. Soc.* **1994**, *116*, 8479–8484.
[24] a) S. Manchineella, T. Govindaraju, *RSC Adv.* **2012**, *2*, 5539–5545; b) T. Govindaraju, M. Pandeeswar, K. Jayaramulu, G. Jaipuria, H. S. Atreya, *Supramol. Chem.* **2011**, *23*, 487–492; c) T. Govindaraju, *Supramol. Chem.* **2011**, *23*, 759–767.
[25] a) T. J. Measey, K. B. Smith, S. M. Decatur, L. M. Zhao, G. L. Yang, R. S. Stenner, *J. Am. Chem. Soc.* **2009**, *131*, 18218–18219; b) Z. Xie, A. Zhang, L. Ye, Z. Feng, *Soft Matter* **2009**, *5*, 1474–1482.
[26] a) D. P. Hong, M. Hoshino, R. Kuboi, Y. Goto, *J. Am. Chem. Soc.* **1999**, *121*, 8427–8433; b) N. H. Andersen, R. B. Dyer, R. M. Fesinmeyer, F. Gai, Z. H. Liu, J. W. Neidigh, H. Tong, *J. Am. Chem. Soc.* **1999**, *121*, 9879–9880; c) A. Jha, S. Narayan, J. B. Udgaonkar, G. Krishnamoorthy, *Biophys. J.* **2012**, *103*, 797–806.
[27] a) A. J. M. Kerrow, E. Buncel, P. M. Kazmaier, *Can. J. Chem.* **1995**, *73*, 1605–1615; b) B. R. Gayathri, J. R. Mannekutla, S. R. Inamdar, *J. Mol. Struct.* **2008**, *889*, 383–393.
[28] J. J. Stewart, *J. Mol. Model.* **2013**, *19*, 1–32.
[29] In variable-temperature ^{1}H NMR spectra of NCDP **1**, the signal of the peripheral phenolic protons showed an upfield shift from $\delta =$ 9.11 ppm to $\delta = 8.84$ ppm due to hydrogen bonding with solvent molecules. Intermolecular hydrogen bonding is ruled out as the distance between the hydrogen-bonding acceptor sites will be >4.0 Å, as revealed by theoretical calculations and the energy-minimized assembled structure.
[30] G. A. Hembury, V. V. Borovkov, Y. Inoue, *Chem. Rev.* **2008**, *108*, 1–73.
[31] R. Dennington, T. Keith, J. Millam, Semichem Inc., Shawnee Mission KS, *GaussView Version 5*, **2009**.
[32] J. J. P. Stewart, Stewart Computational Chemistry, Colorado Springs, CO, USA, *MOPAC2012*, **2012**, 151.
[33] Y. Zhao, D. G. Truhlar, *Theor. Chem. Acc.* **2008**, *120*, 215–241.
[34] M. J. Frisch, G. W. Trucks, H. B. Schlegel, G. E. Scuseria, M. A. Robb, J. R. Cheeseman, G. Scalmani, V. Barone, B. Mennucci, G. A. Petersson, H. Nakatsuji, M. Caricato, X. Li, H. P. Hratchian, A. F. Izmaylov, J. Bloino, G. Zheng, J. L. Sonnenberg, M. Hada, M. Ehara, K. Toyota, R. Fukuda, J. Hasegawa, M. Ishida, T. Nakajima, Y. Honda, O. Kitao, H. Nakai, T. Vreven, J. A. Montgomery, Jr., J. E. Peralta, F. Ogliaro, M. Bearpark, J. J. Heyd, E. Brothers, K. N. Kudin, V. N. Staroverov, R. Kobayashi, J. Normand, K. Raghavachari, A. Rendell, J. C. Burant, S. S. Iyengar, J. Tomasi, M. Cossi, N. Rega, J. M. Millam, M. Klene, J. E. Knox, J. B. Cross, V. Bakken, C. Adamo, J. Jaramillo, R. Gomperts, R. E. Stratmann, O. Yazyev, A. J. Austin, R. Cammi, C. Pomelli, J. W. Ochterski, R. L. Martin, K. Morokuma, V. G. Zakrzewski, G. A. Voth, P. Salvador, J. J. Dannenberg, S. Dapprich, A. D. Daniels, Ö. Farkas, J. B. Foresman, J. V. Ortiz, J. Cioslowski, D. J. Fox, Gaussian 09, Revision C.01, Gaussian, Inc., Wallingford CT, **2009**.
[35] F. L. Weinhold, C. R. Lendis, *Valency and Bonding: A Natural Bond Orbital Donor–Acceptor Perspective*, Cambridge University Press, Cambridge, **2005**.

Received: August 7, 2013
Published online: November 4, 2013

